X-57 Wing Structural Load Testing

Eric J. Miller,[1] Wesley Li,[2] Ashante Jordan[3]
NASA Armstrong Flight Research Center, Edwards, California, 93523, USA

Shun-Fat Lung[4]
Peerless Technologies Corporation, Edwards, California, 93523, USA

The X-57 flight project will provide an opportunity to assess the benefits of distributed electric propulsion. The plan is to use a TECNAM P2006T twin-engine light aircraft (Aeronautiche TECNAM S.p.A., Capua, Italy) as the baseline aircraft, but design and fabricate a new wing to test the technology. The wing when fully integrated onto the X-57 TECNAM P2006T fuselage will incorporate two wingtip cruise electric motors and 12 high-lift electric motors along the wing span. The testing described in this paper confirmed the strength of the X-57 wing for flight and provided an opportunity to calibrate the wing flight strain gages for monitoring loads in flight. The X-57 wing was qualification tested in the National Aeronautics and Space Administration Armstrong Flight Research Center Flight Loads Laboratory. This paper documents the airworthiness approach, test setup, instrumentation, and preliminary results. The X-57 ground load testing lessons learned are also discussed.

I. Nomenclature

AFRC	=	Armstrong Flight Research Center
CG	=	center of gravity
DAS	=	data acquisition system
DEP	=	Distributed Electric Propulsion
DLL	=	design load limit
EQDE	=	EQuation Derivation Program
FEM	=	finite element model
FLL	=	Flight Loads Laboratory
GVT	=	Ground Vibration Test
g	=	acceleration of gravity
HL	=	high lift
IADS	=	Interactive Analysis and Display System
IRIG-B	=	Inter-Range Instrumentation Group
LC	=	load cases
LRT	=	linear resistance transducer
LVDT	=	linear variable differential transformer
MLCS	=	Mechanical Load Control System
Mod	=	modification
NASA	=	National Aeronautics and Space Administration
RMS	=	root mean square
sps	=	samples per second
TC	=	test cases
TRR	=	Test Readiness Review

---

[1] Research Engineer, Aerostructures Branch, AIAA member.
[2] Research Engineer, Aerostructures Branch, AIAA member.
[3] Research Engineer, Aerostructures Branch, AIAA member.
[4] Research Engineer, Aerostructures Branch, AIAA member.

II. Introduction

The National Aeronautics and Space Administration (NASA) Armstrong Flight Research Center (AFRC) (Edwards, California, USA) has an extensive history of ground load testing and flight-testing one-of-a-kind flight research vehicles. The NASA X-57 will be the first all-electric X-plane and will be flown to validate and demonstrate the benefits that distributed electric propulsion (DEP) may yield for the future of aviation. Project personnel are developing a general-aviation-sized electric airplane by modifying an Italian-designed TECNAM P2006T twin-engine light airplane (Aeronautiche TECNAM S.p.A., Capua, Italy). The X-57 development approach is described in Figure 1. Modification (Mod) I consisted of a ground demonstration of the distributed electric propulsion technology on a flatbed truck that traversed an Edwards Air Force Base (Edwards, California, USA) lakebed, and baseline flights of the TECNAM P2006T airplane. Mod II is planned to consist of replacing the gas engines on the baseline TECNAM wing with electric motors and performing flight-testing. The Mod III and Mod IV configurations are planned to be combined into a single effort, with the development consisting of taking the TECNAM P2006T stock wing, which bolts to the top of the fuselage, and replacing it with a new, 32-ft-long, composite wing with two motors with propellers on the wingtips. A dozen electric motors and propellers along the leading edge of the wing would also be incorporated to make up the DEP system.

The X-57 Wing Load Test Team was comprised of personnel from NASA AFRC, the NASA Langley Research Center (Hampton, Virginia), Empirical Systems Aerospace (San Luis Obispo, California, USA) (ESAERO), and Xperimental LLC (San Luis Obispo, California, USA). The X-57 project Prime Contractor, ESAERO, has contracted the Mod III wing design and fabrication to Xperimental. The wing was fabricated at Xperimental and delivered in April 2019 to NASA AFRC for flight instrumentation installation, the wing ground vibration test (GVT), and the wing load test. Figure 2 shows the wing-testing timeline. A pre-test ultrasonic inspection of the wing was conducted upon wing arrival; a post-test ultrasonic inspection was conducted prior to shipping the wing back to ESAERO. Personnel at the NASA AFRC Flight Loads Laboratory installed sensors onto the wing and executed the wing GVT and load test. The wing load test consisted of a qualification test of the wing to 120-percent design load limit (DLL) and a loads calibration of the flight instrumentation located at the wing root. The wing also underwent control surface operational testing to verify control surface freedom of movement while the wing was loaded. These tests were performed to qualify the wing for flight. Data collected during the testing will be used to update models and prepare for flight-testing. Strain gages were mounted internally and externally along the wing to record strain. Inclinometers and string potentiometers were placed at various spanwise locations to measure the deflection of the wing during testing. The wing was transported back to ESAERO in September 2019 for integration of the electric motors and wire harnesses. After integration of the electric motors into the wing, it will be delivered to NASA AFRC for integration onto the TECNAM P2006T airplane.

III. Airworthiness Approach

A conventional airworthiness approach was used for the wing and is shown in Fig. 3. The airworthiness approach required a balance of design, analysis, test, and monitoring techniques to provide an acceptable level of confidence that the wing is ready for flight. Additional discussion on tailoring structural airworthiness requirements can be found in the Armstrong Flight Research Center Structural Airworthiness Guidelines document.[1] The maximum expected load cases were derived based on the expected envelope to meet the project objectives. A total of 19 load cases were developed for analyzing the wing based on maximum expected operating weights, airspeeds, control surface configurations, and gust conditions. There are two ways of approaching the design factor of safety for calculation of structural margins. First, if there were a separate test article that could be taken to failure, then it is reasonable and widely accepted by industry to design using a factor of 1.5 on ultimate. In the case of the X-57, however, there was only one fabricated wing article. A test to failure thus would not be acceptable.

Project personnel chose the second approach: to analyze the wing to a 1.8 factor of safety on ultimate and qualification test the wing to 120-percent DLL to confirm the structural strength beyond the expected flight loads. The qualification test focused on five of the 19 design cases. An additional set of load cases was selected to calibrate the strain-gage instrumentation at the inboard wing station. The test article strains and deflections were monitored during testing to verify that the wing structure was behaving as expected. Inspections are essential for determining the health of the wing prior to and after testing to determine whether any harm to the wing occurred during testing. The X-57 wing has been designed to the maximum expected loads, analyzed to an acceptable factor of safety, and tested to confirm the structural strength. During the flight phase, the inflight shear, bending moment, and torque loads will be monitored at the inboard root station to confirm that the design load cases were within the expected design range. Periodic inspections will be performed to confirm the health of the wing throughout the flight phase. There are multiple ways to tailor an airworthiness approach, but the one utilized was found to be the most suitable for the X-57 project.

IV. Test Objectives

Load testing the X-57 wing allowed the project to meet the following test goals and objectives.

Goal:
1. To demonstrate and validate the structural integrity of the wing for flight.

Objective:
1. Qualification test the wing structure to 120 percent of DLL (normal shear, bending, and torsion);
2. Qualification test the cruise motor mount hard points to 120 percent of DLL (axial in-plane);
3. Produce a database suitable for deriving wing load equations by applying a set of known loads and recording strain-gage outputs (normal shear, normal bending, and torsion), under the consideration that
   o Wing loads will be kept below 100 percent of DLL during flight;
4. Verify that the control surfaces (flaps and ailerons) are free of binding while the wings are loaded to 100 percent of DLL; and
5. Collect wing deflection and strain measurement data for finite element model (FEM) comparison and tuning.

Success Criteria:
1. Qualification and calibration test loads are applied to the wing as specified in the test plan;
2. Data are collected as prescribed in the data acquisition system (DAS) setup worksheet and test Go/NoGos; and
3. Flaps and ailerons are deflected throughout their full range at 100 percent of DLL and any discrepancies in jamming, excessive friction, or excessive deflection are documented.

V. Article Description

The X-57 wing test article is a 379-in span carbon-epoxy wing which was designed and manufactured by Xperimental. The wing has a reference chord of 25.5 in and a total surface area of approximately 9600 in^2. The test article is a straight taper wing with a zero-deg sweep at 70-percent chord. The wing box consists of a main spar, forward spar, and rear spar that extend the full length of the wing. There is an aft secondary spar that is located in the root section that extends the aft wing section to the fuselage attachment points.

Figure 4 shows the wing inverted in the shipping container upon arrival at NASA AFRC. The fuselage is attached to the wing with an aluminum H-frame structure. The H-frame contains four pinned connection points for attaching to the fuselage. The wing contained an aft trailing-edge electric flap that extends from 0 deg to 30 deg. The ailerons are shown on the outboard wingspan. The ailerons are controlled by push rods that attach to a bell crank that is located on the upper surface of the wing. The wing bell crank and the inboard flight-test strain gages are shown in Fig. 5. The cruise and high-lift (HL) nacelles were not available for the loads test so simulators were fabricated to simulate the inertial loads and allow for cruise nacelle thrust loads to be introduced into the wing during the test.

VI. Structural Testing Descriptions

There may be different reasons for performing a load test of a flight structure. The test setup and instrumentation requirements will be highly dependent on the type of test objective. The X-57 testing objectives were targeting a qualification test of the wing and calibration of the strain-gage instrumentation at the wing root. Other types of testing such as proof-testing and model correlation objectives can sometimes be the intent of the testing. A proof or qualification test provides structural strength confidence for airworthiness by subjecting the test article to loads at or above the DLL. A proof test as described in this paper is typically to load levels that could induce failure in the structure. A qualification test is typically a test of the structure to load levels just beyond DLL that maintain the loads in the structure below yield, but high enough to confirm that the structural strength is above the expected in-flight loads. Given that there was only one X-57 wing fabricated, the project chose to perform a qualification test to prevent the wing from being damaged. A proof or qualification test usually requires five or fewer load cases for simple wing geometries. Typically a maximum bending moment and maximum torque case may be sufficient.

A load calibration provides the ability to monitor the loads to verify that the loads are remaining within flight-strength limits and to validate the load predictions made in the analysis of the vehicle structure. Unlike a proof test, a loads calibration may require a dozen or more load cases to collect sufficient loads data. Typically, a wing root or mid-station will be instrumented with shear, bending moment, and torque full-bridge strain gages. Shear gages are located on the wing spar webs and skins, while bending or axial gages are located on the spar caps. Typically, shear gages on the spar webs will assist the shear load calculation. The shear gages on the skin will respond more favorably to wing torque loads. The bending or axial gages on the spar caps will respond to wing bending moment loads. A multi-linear regression is performed using the gage response and the applied loads to calculate load equations for each load component (shear, bending moment, and torque).

The last type of testing corresponds to model correlations. Model correlations are used in conjunction with a proof-loads test, loads calibration test, or to support structural research experiments. The data gained during model correlation testing are used to provide confidence in the analysis model of the test article through FEM validation. There is a wide range to the scope of model correlation exercises. Instrumentation requirements typically are much greater than for a proof-test or load calibration because the goal is to understand the structural behavior in greater detail. Large numbers of strain gages or fiber optic strain sensors are located throughout the structure. The Passive Aeroelastic Test Wing testing conducted at NASA AFRC is good example of this type of testing; more information can be found in Ref. [2]. Strain gages lend themselves well to particular areas of interest, and fiber optics can assist with large global areas such as along the wing span. The X-57 wing test was mainly focused on confirming the wing strength and calibrating loads instrumentation. The team believed that sufficient model correlation could be accomplished with the planned instrumentation.

VII.   Load Case Derivation

The qualification test is used to demonstrate a safety margin for the design and is part of the airworthiness process to show the ability of the wing to withstand the DLL, which consists of the most extreme forces the airplane will ever be expected to encounter during normal flight and ground operations. The airworthiness approach requires that the wing be designed to a factor of safety of 1.8 on DLL and qualification tested to a factor of 1.2 on DLL.

Qualification test loads were applied to the wing surface using 26 vertical actuator load trains. Two vertical actuator load trains were attached at the wing tips (one each side) for applying inertial loads at the cruise motors. Two additional horizontal actuator load trains were attached at the wing tips (one each side) for applying thrust loads at the cruise motors. The high lift motor inertia weights were simulated using shot bags. The qualification test loads distribution were designed to match the shear, bending, and torque DLL envelope. Figure 6 shows the pad layout and load cell locations on the wing.

A. Design Limit Loads

A total of 19 design flight load cases have been developed. The design loads for flight consist of aerodynamic, motor inertial loads, and motor thrust loads. The wing inertia acts as load alleviation for maneuver load cases and was ignored (to be conservative) in the original design load cases; however, it was important to consider the mass of the engines (tip and high-lift engines) since the center(s) of gravity (CG) of these masses are located forward of the wing leading edge and elastic axis and have significant impact on the wing torsion calculation.

The aerodynamic loads were calculated based on the 3000-lb airplane. These load cases included positive and negative acceleration of gravity (g) maneuver, gust, rolling, asymmetric flight, and flap retracted or extended conditions within the design flight envelope at sea level and 15,000 ft altitude. Five critical design load cases plus a ground case were selected for qualification test. These six critical design load cases included the expected maximum shear, maximum bending moment, maximum torsion and maximum cruise motor thrust cases.

B. Design Net Loads (Design Load Cases with Wing Inertia)

The design loads were refined further to accurately represent the loads on the wing structures by adding the expected wing inertia. The wing inertial loads were derived from the FEM mass distribution. The FEM was created directly from the computer aided design (CAD) and fabrication drawings of the wing. The net design loads were equal to the summation of aerodynamic loads, flight wing inertia, HL assembly inertia, and cruise assembly inertia. The target qualification test loads were equal to 120 percent of the net design loads. The calculation of the test loads is described in Eqs. (1) and (2).

$$\begin{aligned} &(100\% \text{ Design Net loads}) = \\ &(\text{Aerodynamic Loads}) + (\text{Inertia Flight Wing}) + (\text{Inertia Flight HL}) + (\text{Inertia Flight Cruise}) \end{aligned} \tag{1}$$

$$\begin{aligned} &(\text{Target qualification test loads}) = \\ &(120\% \text{ Design Net Load}) = 1.2 * (100\% \text{ Design Net Load}) \end{aligned} \tag{2}$$

C. Qualification Test Pad Loads

To calculate the qualification test pad load, the test wing inertia weights were subtracted from the design net loads. Some components, such as cruise nacelle, HL assemblies, instrumentation, and traction or power cables were missing; it is important to account for all the missing inertial loads in the qualification test.

The test wing inertia and test motor inertias were summed together to get the total wing inertia for qualification test. The test wing inertia was fixed and was under 1.0 g. The test motor inertia weights varied based on the load case.

Shot bags were used to simulate the motor inertia. Eqs. (4), (5), and (6) show the calculation of the 60-percent, 100-percent, and 120-percent qualification test loads.

$$
\begin{aligned}
&(60\% \text{ Qual Test Loads}) = \\
&(60\% \text{ Net Design Loads}) - (100\% \text{ Inertia Test Wing}) - \\
&(60\% \text{ Inertia Test HL}) - (60\% \text{ Inertia Test Cruise})
\end{aligned}
\tag{4}
$$

$$
\begin{aligned}
&(100\% \text{ Qual Test Loads}) = \\
&(100\% \text{ Net Design Loads}) - (100\% \text{ Inertia Test Wing}) - \\
&(100\% \text{ Inertia Test HL}) - (100\% \text{ Inertia Test Cruise})
\end{aligned}
\tag{5}
$$

$$
\begin{aligned}
&(120\% \text{ Qual Test Loads}) = \\
&(120\% \text{ Net Design Loads}) - (100\% \text{ Inertia Test Wing}) - \\
&(120\% \text{ Inertia Test HL}) - (120\% \text{ Inertia Test Cruise})
\end{aligned}
\tag{6}
$$

Once the qualification test loads were calculated, the pad loads at each wing station were calculated by matching the design shear loads and bending moment envelope. The torsion loads were then calculated by solving for the forward and aft pad load at each station based on the pad distance from the torsion axis.

To reduce the risk of overloading the wing and wing surface skin, the maximum shear generated by the pad at each station was limited to the 120-percent design loads and the pad maximum pressure was limited to 15 psi. The qualification test pad loads of case 8, one of the critical load cases, are shown in Figs. 7, 8, and 9. The pad shear load envelopes (shown in red in the figures) were limited by the 120-percent design shear loads (shown in black in the figures). The qualification test shear cannot exceed the design loads at each station. Due to the limited pad distribution, the qualification test shear loads at the inboard station were lower than the design load. Figures 7, 8, and 9 show that the loads (shear, bending, and torsion, respectively) at the inboard station (~17 in) are lower than the design loads and the expected in-flight loads. Table 1 shows the actuator load case summary for the X-57 load testing. The team settled that these qualification loads were sufficient to support the flight phase and meet project objectives. During the flight phase, in-flight shear, bending moment, and torque loads will be monitored to ensure that the loads do not exceed 100 percent of DLL at the inboard root station.

Table 1. Load case definition.

Case Description Load (lbs)	Design Case	Load Factor	LCUP6fnt	LCLP6a	LCLP6f	LCLP5a	LCLP5f	LCLP4a	LCLP4f	LCLP3a	LCLP3f	LCLP2a	LCLP2f	LCLP1a	LCLP1f	LCRP1f	LCRP1a	LCRP2f	LCRP2a	LCRP3f	LCRP3a	LCRP4f	LCRP4a	LCRP5f	LCRP5a	LCRP6f	LCRP6a	LCRP6fnt
Positive Bending (60%DLL)	8	0.6	100	175	100	175	200	139	259	139	286	125	325	120	230	230	120	325	125	286	139	259	139	200	175	100	175	100
Max Torsion (60%DLL)	9	0.6	70	168	70	176	199	208	208	218	218	230	230	234	126	126	234	230	230	218	218	208	208	199	176	70	168	70
Negative Bending (60%DLL)	10	0.6	0	0	-5	0	-113	0	-125	0	-133	0	-125	0	-90	-90	0	-125	0	-133	0	-125	0	-113	0	-5	0	0
Positive Bending (60%DLL)	11	0.6	150	85	150	113	177	121	204	139	201	133	227	120	155	218	132	271	179	193	222	178	207	175	175	25	175	25
Positive Bending (60%DLL)	12	0.6	0	175	0	178	72	207	78	222	88	237	93	225	25	137	113	199	131	177	133	243	22	160	0	100	0	100
Calibration Case	a	NA	0	0	0	0	0	0	0	0	0	460	460	468	252	252	468	460	460	0	0	0	0	0	0	0	0	0
Calibration Case	c	NA	0	0	0	0	0	0	415	415	435	435	0	0	0	0	0	0	0	0	435	435	415	415	0	0	0	0
Calibration Case	f	NA	140	336	140	353	398	0	0	0	0	0	0	0	0	0	0	0	0	0	0	0	0	398	353	140	336	140
Calibration Case	g	NA	0	0	0	0	0	0	0	0	0	435	0	460	0	252	252	0	460	0	435	0	0	0	0	0	0	0
Calibration Case	i	NA	0	0	0	0	0	0	0	435	0	460	0	468	0	0	468	0	460	0	435	0	0	0	0	0	0	0
Positive Bending (100%DLL)	8	1.0	167	292	167	292	333	231	431	232	476	208	542	201	383	383	201	542	208	476	232	431	231	333	292	167	292	167
Max Torsion (100%DLL)	9	1.0	117	280	117	294	331	346	346	363	363	383	383	390	210	210	390	383	383	363	363	346	346	331	294	117	280	117
Negative Bending (100%DLL)	10	1.0	0	0	-8	0	-188	0	-208	0	-221	0	-208	0	-150	-150	0	-208	0	-221	0	-208	0	-188	0	-8	0	0
Positive Bending (100%DLL)	11	1.0	250	142	250	188	296	202	339	231	335	222	378	200	258	364	220	451	299	322	370	296	345	292	292	42	292	42
Positive Bending (100%DLL)	12	1.0	0	292	0	296	121	345	130	370	147	394	156	375	42	228	189	332	218	295	221	405	36	267	0	167	0	167
Positive Bending (120%DLL)	8	1.2	200	350	200	350	400	278	517	279	571	250	650	241	459	459	241	650	250	571	279	517	278	400	350	200	350	200
Max Torsion (120%DLL)	9	1.2	140	336	140	353	398	415	415	435	435	460	460	468	252	252	468	460	460	435	435	415	415	398	353	140	336	140
Negative Bending (120%DLL)	10	1.2	0	0	-10	0	-225	0	-250	0	-265	0	-250	0	-180	-180	0	-250	0	-265	0	-250	0	-225	0	-10	0	0
Positive Bending (120%DLL)	11	1.2	300	170	300	225	355	243	407	278	402	266	454	240	310	436	264	541	359	386	444	356	414	350	350	50	350	50
Positive Bending (120%DLL)	12	1.2	0	350	0	355	145	414	156	444	176	473	187	450	50	273	227	398	262	354	266	486	44	320	0	200	0	200

VIII. Pre-Test Predictions

To ensure the load test ran smoothly without damaging the wing, a FEM was created to provide better understanding of the behavior of the wing under various loading conditions. The pre-test predictions were also used in the design of the actuator load trains to ensure there was enough actuator stroke throughout the entire deflection range of the wing. The wing FEM model contained 1,484,736 nodes and 962,289 elements generated from MSC/NASTRAN (MSC Software Corporation, Newport Beach, California, USA) [3] as shown in Fig. 10. The load

pads with Rubberlite Neoprene foam (part number SCE43B) (Rubberlite Incorporated, Huntington, West Virginia, USA) material were also modeled using contact elements for a more accurate pad pressure simulation. The connection between the wing and the test stand was modeled using spring elements to simulate the fuselage stiffness. These spring constants were estimated from the full aircraft FEM model utilizing the MSC/NASTRAN inertial relief linear static solution procedure by using the free vehicle to react the applied load. Cruise motors and high-lift motors were modeled as lumped mass.

There were five calibration load cases and five envelope load cases, as defined in Table 1. The calibration load cases were for load equation calibration purposes; the envelope load cases were for maximum shear, bending moment, and torque qualification testing. The same five envelope load cases were applied in the 60-percent, 100-percent, and 120-percent level of DLL in order to be able to monitor the wing deflection easily and reduce the risk of damage to the wing. The strain output from the FEM model was in the element axes. The strain output location and direction taken from the FEM model was based on the strain-gage location and orientation. Typical load case definitions are shown in Table 1. The corresponding deflections from the finite element model are shown in Figure 11. The failure index based on maximum strain theory are listed in Table 2 for evaluating the extra margin in the wing during loading.

Table 2. Maximum failure index with respect to load cases.

Case description Load, lb	Design case	Failure index
Positive bending (60% DLL)	8	0.282
Maximum torsion (60% DLL)	9	0.304
Positive bending (60% DLL)	11	0.252
Positive bending (60% DLL)	12	0.239
Calibration case	a	0.210
Calibration case	c	0.228
Calibration case	f	0.322
Calibration case	g	0.142
Calibration case	i	0.262
Positive bending (100% DLL)	8	0.459
Maximum torsion (100% DLL)	9	0.496
Positive bending (100% DLL)	11	0.411
Positive bending (100% DLL)	12	0.387
Positive bending (120% DLL)	8	0.547
Maximum torsion (120% DLL)	9	0.591
Positive bending (120% DLL)	11	0.489
Positive bending (120% DLL)	12	0.461

IX. Test Setup

The test setup includes a test rig for restraining the wing to the floor of the Flight Loads laboratory. A wing load test fixture was provided by Pyramid Space Inc. (Carlsbad, California, USA) for constraining the wing to the floor. The test fixture was designed to a factor of safety of 3.0 based on the applied test loads. The X-57 wing test setup is shown in Fig. 12. The test rig utilized spring washers at the interface attachment points for simulating the fuselage stiffness. Figure 13 shows the wing mount attachment and the spring washer configuration. The spring stiffness was derived from the FEM of the fuselage. Spring washers of various stiffness were combined to match the required FEM stiffness. The spring assemblies were tested in the FLL load frame to verify the stiffness.

An aileron actuation rig was located in front of the wing for actuating the aileron bell crank located on top of the wing surface. The ailerons were actuated during the 100-percent DLL load testing to check for binding in the actuation system. The two arms were connected to the bell crank on the top surface of the wing using cables with 500-lb inline load cells. An engineer actuated the green levers to move the ailerons during 100-percent load while watching a display of aileron deflection and cable load. An electric controller was provided for the X-57 flap actuation. The controller was powered by a benchtop power supply.

The main cruise motors for the X-57 are attached at the wing tips. The loads test utilized mass simulators attached to the wing tips. Figure 14 shows the wing cruise motor and high-lift motor simulators. The cruise simulators allowed project personnel to apply thrust loads to the wing tip and vertical download at the simulator CG to simulate inertial loads during upload testing. The total weight of the cruise simulator was approximately 134 lb. The mass simulators consisted of three parts: a flat plate that is attached to the wing tip, an aluminum tube that attaches to the flat plate, and steel ballasts secured inside the aluminum tube. There was a clevis attachment on the bottom of the tube, as well as on the forward, front of the tube. The cruise thrust loading support structure allowed a thrust load to be applied to the cruise simulator. The maximum axial applied load was 456 lb. A load cell at the actuator and an inline load cell at the cruise simulator attachment were used. A string potentiometer was added during testing to measure the in-plane deflection of the wing during cruise simulator axial loading. The wing also contained 12 high-lift simulators (six per side) that were cantilevered off the leading edge of the wing. The high-lift simulators each weighed 15 lb; additional dead weight was applied to account for the high-lift nacelle inertias.

A total of 26 load pads were used at 12 loading stations, six on each wing. The load pads included an aluminum backing plate with foam contact pad bonded to it, and are designed to evenly distribute the point load from the hydraulic actuators. Load cells were attached to the bottom of the load pads to provide feedback to the load control system and record the applied loads. The hydraulic actuators were secured to the FLL floor track using I-beams, jack bases, and pedestals. The hydraulic actuators were used to generate uploads for testing. Four additional actuators (two per side) were attached at the wing tips for applying inertial and thrust loads at the cruise motors.

The 80-channel Mechanical Load Control System (MLCS) was used to supply mechanical loads at 30 locations on the wing. The MLCS was programmed to control the load control channels, which corresponded to the load pad locations on the wing. Seven hydraulic control carts were used to supply hydraulic pressure to the actuators. Load feedback to the MLCS was provided by force transducers located on top of each actuator.

The FLL DAS was used to collect strain, load, deflection, and inclinometer data. Data were collected at 100 samples per second (sps) and time synchronized to IRIG-B time. The data file was then decimated to 20 sps and exported for post-test processing. The FLL utilizes the Interactive Analysis and Display System (IADS) to display real-time data broadcast by the DAS. Three IADS stations were required to support test operations. One IADS station was for the Test Conductor, another for the Test Director, and the third for the Load Controller workstation. The IADS data were recorded at 20 sps and time synchronized to IRIG-B time. The FLL wireless communication system used 15 wireless headsets to enable communication between test personnel during test operations. Three mobile digital video cameras were positioned in the test setup to monitor test operations. Selected video recordings were delivered for post-test documentation.

To produce the down load weight, 25-lb shot bags and 5-lb shot bags were placed on top of the wing in dedicated zones. The shot bags were stacked to achieve the total load, and were placed in increments of 60 percent, 100 percent, and 120 percent of the total load.

X. Instrumentation

The X-57 load test included load cells, linear resistance transducers (LRTs), linear variable differential transformers (LVDTs), inclinometers, and string potentiometers. Figure 15 highlights the instrumentation used during the test; Table 3 lists the instrumentation data channels. A total of 30 load cells were used to measure the loads that were applied to the wing. The load cells were dual-bridge force transducers with one bridge connected to the MLCS for load control and the other to the DAS for data. A total of 26 load cells were used for the load pads. Two load cells were used for measuring the vertical inertial loads applied to the wingtip cruise simulators. Two load cells were used for measuring the applied axial thrust load to the wingtip cruise simulators. Four load cells were used for data monitoring purposes. Two load cells were located at the wingtip cruise simulator in line with the axial cable. Two load cells were collinear with the bell crank actuator cables.

Table 3. Instrumentation data channels.

Channel type	Units	Number
Quarter-bridge ground-test strain gages	microstrain	36
Full-bridge flight-test strain gages	mV/V	34
Actuator load cells	lbf	30
Cruise thrust load inline load cell	lbf	2
Aileron bell crank inline load cell	lbf	2
Deflection potentiometers	in	18
LVDTs	in	9
Actuator LRTs	in	30
Inclinometers	deg	12

Each actuator was fitted with an LRT, which measures the stroke of the actuator. Knowing the stroke of the actuator is important for safety of test and also provides another measurement of wing displacement. There were a total of 30 LRTs. The LRT data were displayed on both the MLCS and DAS systems. Nine LVDTs were positioned to measure the displacement of the spring washer mounts in the X and Y direction during wing loading. One LVDT was used to measure the vertical displacement of the test article during wing loading. Twelve inclinometers were used to measure wing twist and control surface deflection angles. Sixteen string potentiometers were used to measure the wing deflection. Two string potentiometers measured in-plane wing deflection at the wing tips. Full-bridge and quarter-bridge axial metallic foil strain gages were used for this test. The full-bridge gages are thermally compensated and thus were used for flight loads monitoring. A total of 34 full-bridge channels (17 per side) were installed. The bridges were installed on the wing spars, caps, and wing skins from approximately 17in to 23 in wing span. The goal is to sense the shear, bending, and torque loads transferring into the wing root. Axial gages were used for monitoring the strains on the ground and for subsequent model correlation activities. The test conditions maintain constant temperature throughout the load profile, thus not requiring the thermal compensation of full bridges. Axial gages provided a uniaxial strain that can be easily compared to the FEM.

XI. Test Summary

Load testing began in mid-August 2019 and ended in early September of the same year. Table 4 shows the test sequence of all of the load cases that were executed. The project began with a lower-level shot-bag loading test and worked up in load values until reaching the 120-percent DLL cases. The calibration cases used a subset of the actuators, allowing project personnel to assess the wing response with the minimal numbers of actuators but utilizing maximum load pad values to assess load train and pad response. The 60-percent DLL cases were the first time all the actuators were used. These cases were also the first time the wing actuators were pushing up and the wingtip actuator was pulling down on the wingtip to simulate the inertial load. The electric flap was actuated during the 60-percent DLL testing to check for binding. The 100-percent load cases and then 120-percent load cases were completed. The aileron was actuated at 100 percent of DLL. Figure 16 shows the X-57 wing hydraulic upload testing.

Table 4. Test sequence.

Load sequence	Hydraulic or shot bag	Flap check	Aileron check
2-g Inertia landing, 120% shot bag	Shot bag		
Cruise Case, 120%	Hydraulic		
2-g Inertia landing, 120% w/cruise	Shot bag + hydraulic		
Cal, a	Hydraulic		
Cal, c	Hydraulic		
Cal, g	Hydraulic		
Cal, i	Hydraulic		
#8, 60%	Hydraulic	Yes	
#9, 60%	Hydraulic	Yes	
#11, 60%	Hydraulic	Yes	
#11, 60%	Hydraulic	Yes	
#8, 60%	Hydraulic	Yes	
#8, 60% - w/cruise	Hydraulic	Yes	
#12, 60%	Hydraulic	Yes	
#12, 60%	Hydraulic	Yes	
#8, 60%	Hydraulic	Yes	
#8, 100%	Hydraulic		Yes
#9, 100%	Hydraulic		Yes
#11, 100%	Hydraulic		Yes
#11, 100%	Hydraulic		Yes
#12, 100%	Hydraulic		Yes
#12, 100%	Hydraulic		Yes
#8, 120%	Hydraulic		
#8, 120% - w/cruise	Hydraulic		
#9, 120%	Hydraulic		
#11, 120%	Hydraulic		
#11, 120%	Hydraulic		
#12, 120%	Hydraulic		
#12, 120%	Hydraulic		
Cruise case, 120%	Hydraulic		
#10, 60% shot bag	Shot bag		
#10, 100% shot bag	Shot bag		Yes
#10, 120% shot bag	Shot bag		
#8, 60%	Hydraulic		
#9, 60%	Hydraulic		
#9, 60% - w/cruise	Hydraulic		

Before actual load testing could begin, the team performed an operation called dump tuning. During dump tuning, a subset of the actuators were taken to a load level of approximately 10 percent and then system was instantly depressurized. Dump tuning simulated what would happen in the event of the hydraulics losing power or requiring emergency shutdown. The reason for dump tuning was to determine how the load reduced in the actuators. The goal is for the outboard actuators to reduce in load before the inboard actuators, to protect the wing from an excessive load. The tuning aspect is adjusting the dump valves on the hydraulic carts from fully closed, to slightly open, and all the way up to fully open. The basic premise is to have the inboard dump valves closed and vary in setting all the way out

to fully open at the wingtip. This state is accomplished with just a few inboard actuators and increasing to all actuators. The team watched the load dissipation during the event, and, if results were sufficient, the team added more actuators for the next test. Maintaining a constant hydraulic cylinder bore diameter for all actuators is required to obtain satisfactory results.

A typical test day began with a crew briefing to discuss the activities of the day. Due to the large number of actuators, the setup to place all 30 actuators on the wing took almost two hours in the beginning, but toward the end of testing took approximately an hour and a half. A load profile was run one or two times. Actuator pacing was initiated during the earlier runs, which prompted the team to continually increase the time dedicated to the load profiles and helped improve the data quality. Actuator pacing is initiated by the load controller when one actuator falls behind the others. When pacing is initiated, the controller slows down all of the actuators.

Two smaller shot-bag download cases were executed early in testing. The largest shot-bag download case, case 10, was executed toward the end of testing, allowing the team to build confidence in the wing strength before loading the wing to its limits with people in near proximity. Figure 17 shows the X-57 wing shot-bag download testing at maximum load.

Figure 18 shows the X-57 wing hydraulic upload testing from the display station point of view. In the figure, the test director and test conductor are monitoring the IADS displays as the wing is loaded. Sitting near the wing allowed the team to listen to the wing for popping or cracking sounds; various noises emanating from the structure could indicate local damage. The wing was silent throughout all testing.

During testing the deflection and strain data were compared to predictions. The test deflections were approximately 20 percent higher than those predicted by the FEM. The important thing is that there was still enough actuator stroke to complete the test. Figure 19 shows the X-57 wing FEM-predicted displacements compared with test results for load case 8. Strains from axial strain gages installed along the wing main spar upper and lower surface were also monitored. Figure 20 shows the X-57 wing FEM-predicted axial strain compared with test results for load case 8. A less than 20-percent difference was observed for the outboard strain gages, but the two inboard locations showed larger inconsistencies. The team plans to assess this condition as they update the FEM models. The load path near the wing root is somewhat complicated due to the fact that the loads must transfer from the main spar to the forward and aft spars and then into the H-frame. The complex load paths at the root also effected the wing flight strain gages, but in the end did not significantly affect the results for the load equations.

XII. Load Equation Results

The project plans to monitor the wing root shear bending moment and torque loads in flight to verify that the loads stay below the design limits. The load calibration method developed by Skopinski and Aiken is found in Ref. [4]. The NASA AFRC FLL has conducted multiple load calibrations; a few examples are found in Ref. [5]. A program referred to as the EQuation Derivation Program (EQDE), a NASA AFRC in-house linear regression analysis program, was used for deriving load equations for monitoring shear, bending, and torque loads. The EQDE calculates the strain-gage influence coefficients and other statistical information for each load condition selected. The EQDE also derives the coefficients for a given combination of strain-gage bridges based on the analysis of the data. The EQDE computes the root mean square (RMS) of the fit of the derived load equation to the test data and ranks the order of the derived equations, as shown in Eq. (8).

$$\text{EQDE RMS error} = \sqrt{\frac{\sum_{t=1}^{n}(Derived\ load_i - Measured\ load_i)^2}{\sum_{t=1}^{n}(Measured\ load_i)^2}} \qquad (8)$$

Check cases were used to indicate how well the derived loads equation can calculate loads for load cases from which they are not derived. The check-case verification helps understand how the loads equations will perform with flight data, as shown in Eq. (9).

$$\text{Check-case RMS error} = \sqrt{\frac{\sum_{t=1}^{n}(Derived\ load_i - Check\ load_i)^2}{\sum_{t=1}^{n}(Check\ load_i)^2}} \qquad (9)$$

Not all of the strain gages used in the wing loading test were used in the derivation of the load equations. For flight-testing of the X-57 only a subset of the strain gages will be monitored. Figure 5 shows the wing bell crank and inboard flight-test strain gages. A subset of the wing test cases were used in the derivation for real-time flight loads. Eleven of the wing qualification test cases were used in the strain-gage derivation. The load cases were based on the 120-percent wing qualification test cases. Each wing was calibrated separately using 17 full-bridge strain gages per wing for the calculations; see Table 5. The data for the calibration load profile were clipped for each load case and were set aside to be used as the calibration cases. Table 6 lists the results for the four strain-gage-derived load cases

for the shear, bending moment, and torque equations for load case 9. An initial review of the load equations show that each equation is using a combination of the shear, bending moment, and torque strain gages, which should be expected because the ideal equation is calculating the pure load but also correcting the equation for influence from the other two effects. The shear load equation should be expected to contain shear strain gages, but also possibly bending or torque strain gages, or both, to remove the bending or torque influence from the shear equation. The calibration errors and the errors calculated from just the check cases are listed for each load equation. The worst check-case error is 8.51 percent, which is similar to past experience based on Ref. [4].

Table 5. List of strain gages.

# of gages	Left strain gage	Right strain gage
1	LWS023fs	RWS023fs
2	LWS017ms	RWS017ms
3	LWS017rs	RWS017rs
4	LWB023fsu	RWB023fsu
5	LWB023fsl	RWB023fsl
6	LWB017msu	RWB017msu
7	LWB017msl	RWB017msl
8	LWB017rsu	RWB017rsu
9	LWB017rsl	RWB017rsl
10	LWT017fsu	RWT017fsu
11	LWT017fsl	RWT017fsl
12	LWT017rsu	RWT017rsu
13	LWT017rsl	RWT017rsl
14	LWRB014msu	RWRB014msu
15	LWRB014msl	RWRB014msl
16	LWRB014rsu	RWRB014rsu
17	LWRB014rsl	RWRB014rsl

Legend: LW: left wing; RW: right wing; S: shear; B: bending; T: torsion; RB: rib; fs: front spar; ms: main spar; rs: rear spar; u: upper; l: lower.

Table 6. Strain-gage load equation error for case 9, 120 percent.

	GAGE ID				EQDE RMS ERROR, %	Check RMS ERROR, %
Left wing shear	LWS023fs	LWS017ms	LWS017rs	LWRB014msl	2.21	4.29
Left wing bending	LWS023fs	LWS017ms	LWB017rsl	LWT017fsl	2.24	5.56
Left wing torsion	LWT017fsl	LWT017rsu	LWT017rsl	LWRB014rsu	3.70	7.92
Right wing shear	RWS023fs	RWS017ms	RWB017rsu	RWRB014msu	2.60	8.51
Right wing bending	RWS023fs	RWB017rsl	RWT017fsl	RWT017rsu	2.40	6.33
Right wing torsion	RWS017ms	RWB017msl	RWT017fsl	RWRB014msl	3.43	7.16

Legend: LW: left wing; RW: right wing; S: shear; B: bending; T: torsion; RB: rib; fs: front spar; ms: main spar; rs: rear spar; u: upper; l: lower.

XIII. Conclusions

The X-57 Wing was qualification tested in the National Aeronautic and Space Administration Armstrong Flight Research Center Flight Loads Laboratory (FLL). A conservative time tested loading and monitoring methodology was used, which led to a successful test meeting all the test objectives. The wing when fully integrated onto the X-57 fuselage will incorporate two wingtip cruise electric motors and 12 high-lift electric motors along the span. A total of 28 hydraulic cylinders were used to apply combinations of shear, bending, and torque loads to the wing. Two additional hydraulic cylinders applied axial thrust loads to the wing tips. The innovative part of this test was the ability to apply upload to the wing while at the same time pulling down on the wingtips to simulate the cruise nacelle inertial loads. This test was the largest test to date in terms of actuator count using the FLL Mechanical Load Control System. The applied loads were 120 percent of design load limit. The wing attained a maximum deflection at the wing tips of 13 in, which was approximately 20 percent higher than what was predicted by the finite element model. The ailerons and flaps were actuated throughout their full range of travel during maximum loading. The team was also successful in simulating the fuselage attachment stiffness using spring washers at the four wing attachment points. This method allowed the wing loads to distribute as they would in the actual fuselage. The testing described in this paper confirmed the strength of the wing for flight and provided an opportunity to calibrate the wing strain gages for monitoring loads in flight. This paper documents the airworthiness approach, test setup, instrumentation, and preliminary results. The X-57 ground load testing lessons learned are also discussed.

References

[1] Armstrong Flight Research Center Research Engineering Directorate, "Aircraft Structural Safety of Flight Guidelines," AFG-7123.1-001, Baseline-5, expires April 1, 2020.

[2] Pena, F., *Fiber-Optic Strain-Based Deflection and Twist Sensing for a High-Aspect-Ratio Swept Wing,* NASA/TM-2020-220465, 2020.

[3] MSC Software Corporation, Newport Beach, California, www.mscsoftware.com [accessed March 25, 2020].

[4] Skopinski, T. H, Aiken, W. S., Jr., and Huston, W. B., *Calibration of Strain-Gage Installations in Aircraft Structures for the Measurement of Flight Loads,* NACA-TR-1178, 1954.

[5] Jenkins, J. M., and DeAngelis, V. M., *A Summary of Numerous Strain-Gage Load Calibrations on Aircraft Wings and Tails in a Technology Format,* NASA TM 4804, 1997.

Figures
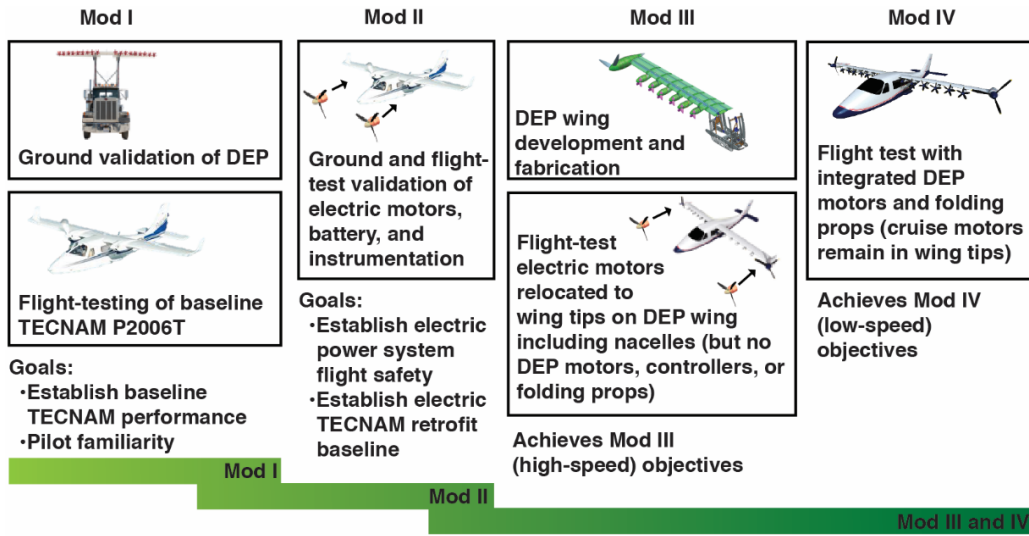
Fig. 1. The development of the X-57 airplane.
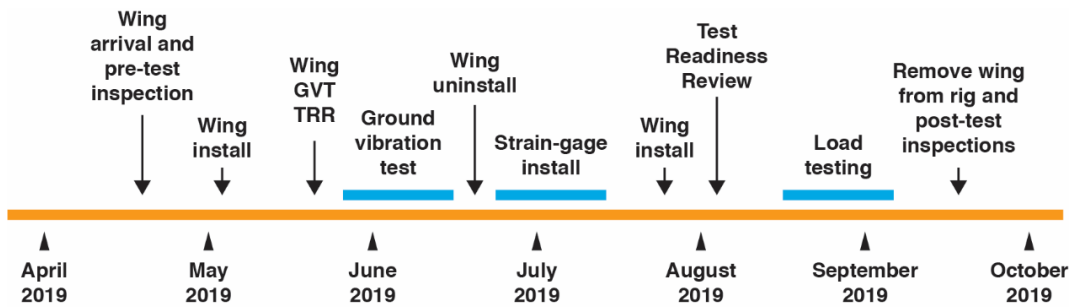
Fig. 2. The X-57 wing-testing timeline (the blue bar represents task duration).
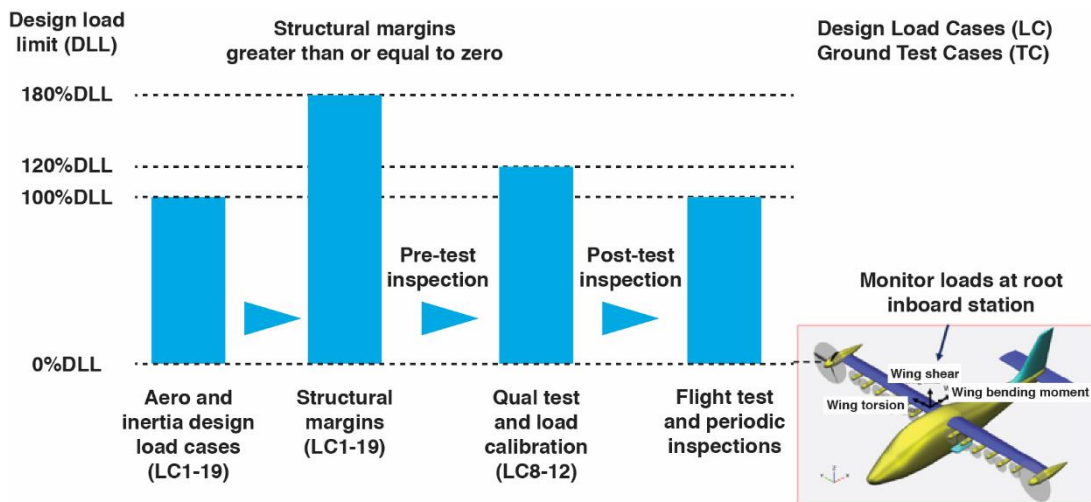
Fig. 3. The X-57 conventional airworthiness approach.

13
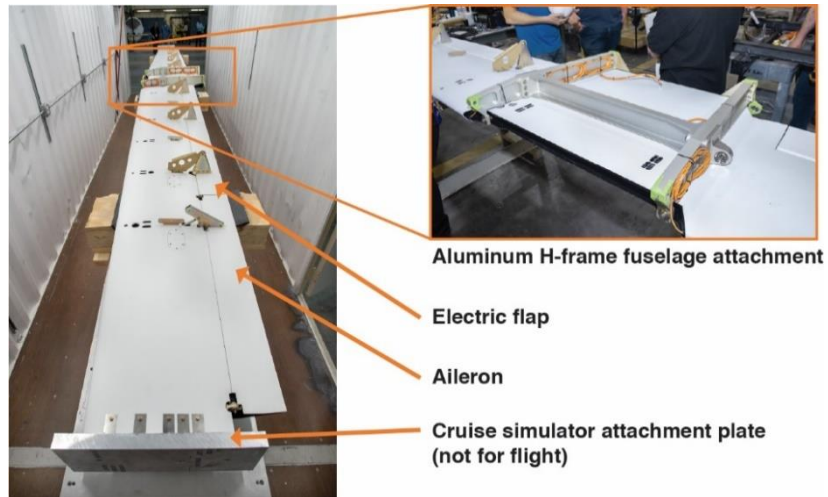
Fig. 4. The X-57 wing inverted in the shipping container.

Fig. 5. Wing bell crank and inboard flight-test strain gages.
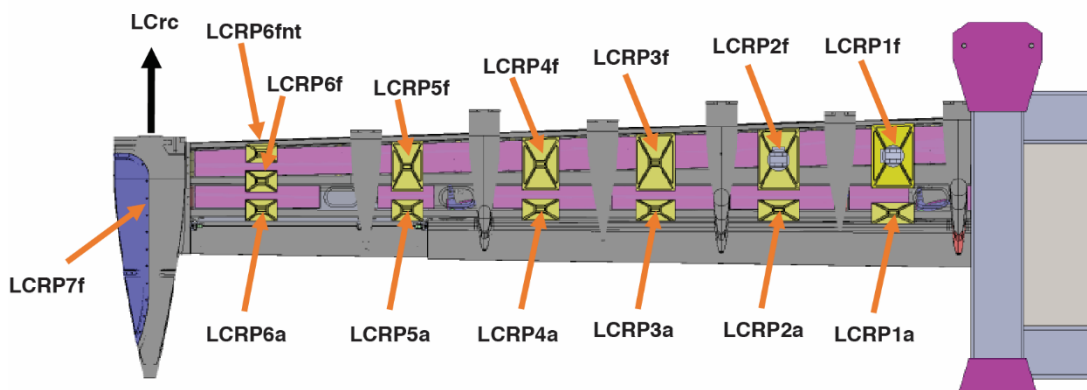
Fig. 6. The X-57 wing load pad and load cell configuration.
Legend: LC: load cell; RP: right wing pad; f: front pad; a: aft pad; fnt: far forward pad; and rc: right cruise.

Shear distribution
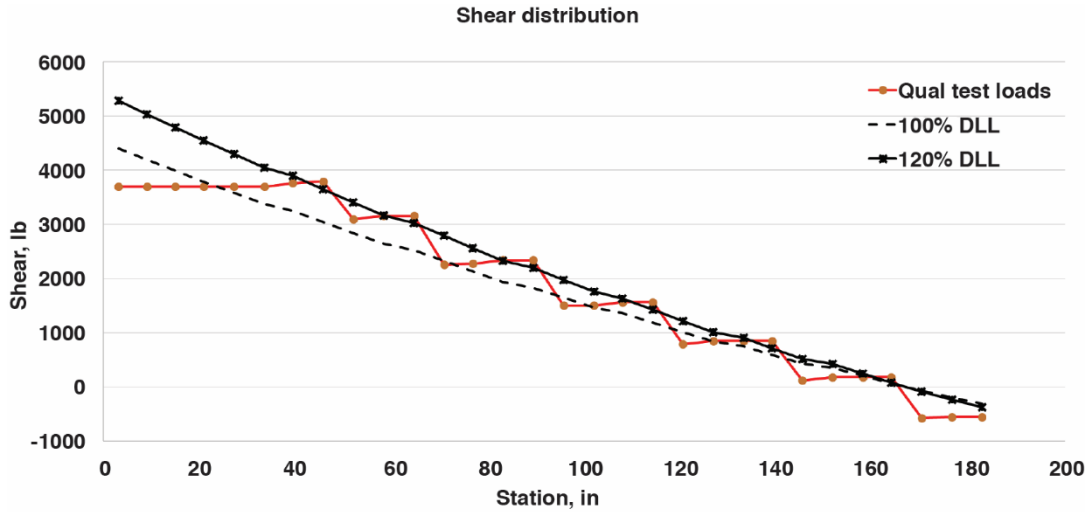
Fig. 7. Shear load distribution.

Bending moment distribution
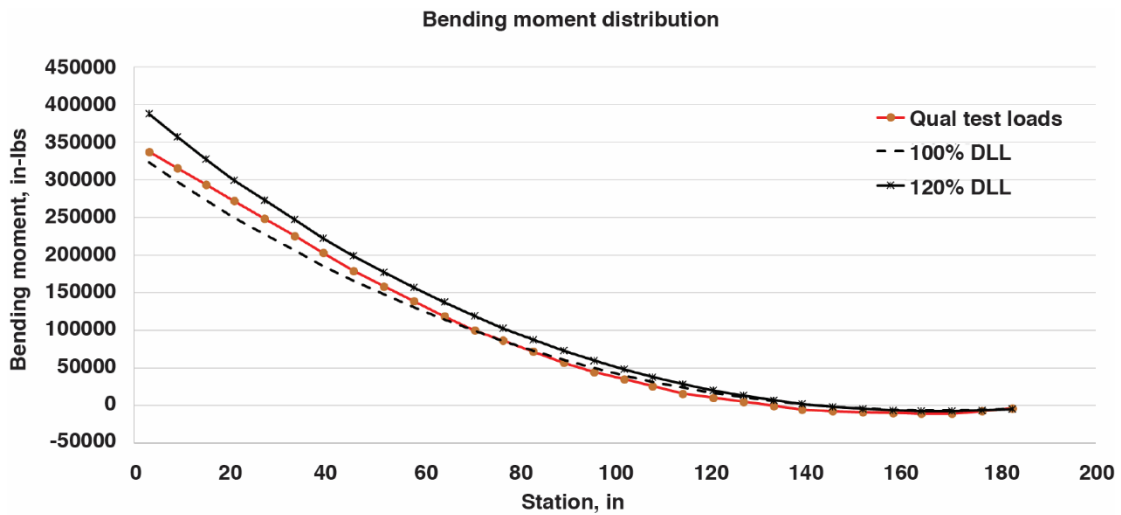
Fig. 8. Bending moment distribution.

Torsion distribution
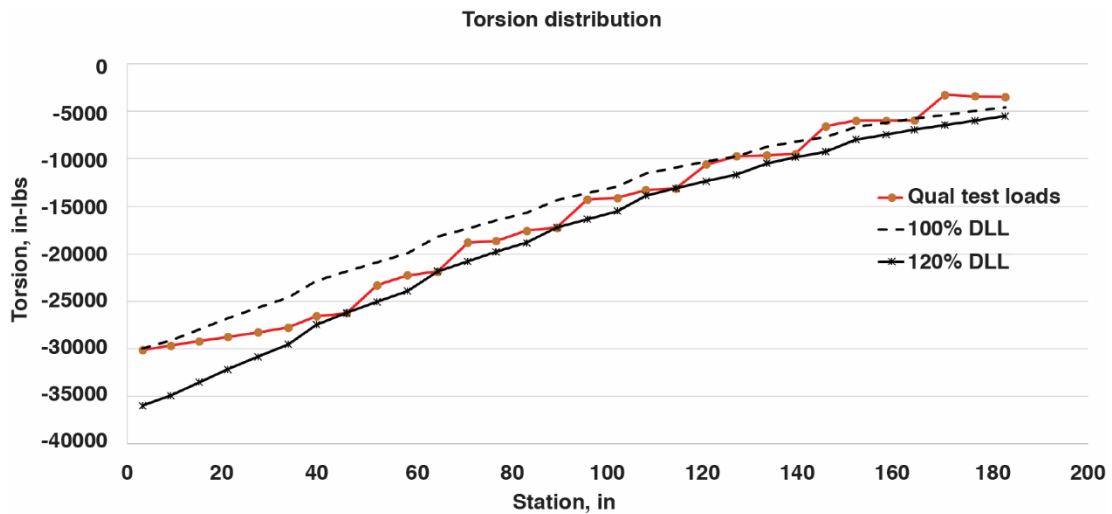
Fig. 9. Torsion distribution.
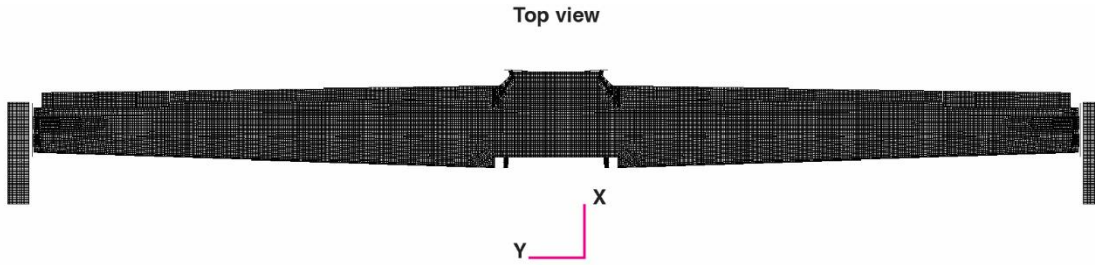
Fig. 10. The finite element model of the X-57 wing.
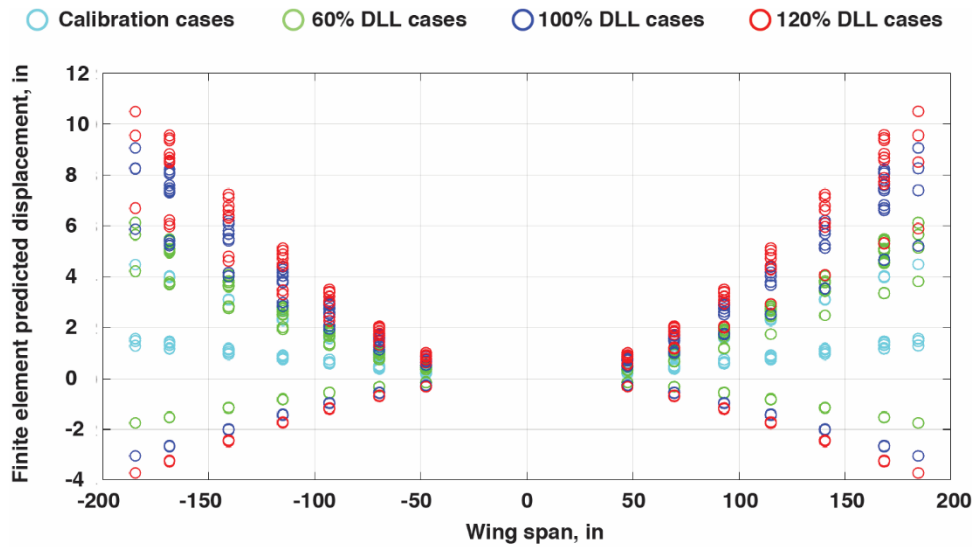
Fig. 11. The X-57 wing finite-element-model-predicted displacements.
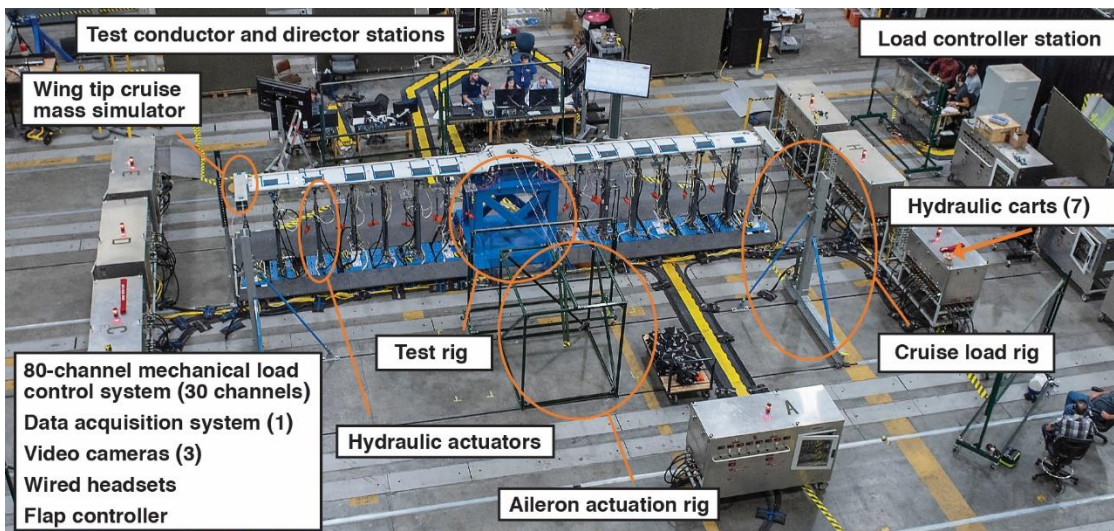
Fig. 12. The X-57 wing test setup.

16
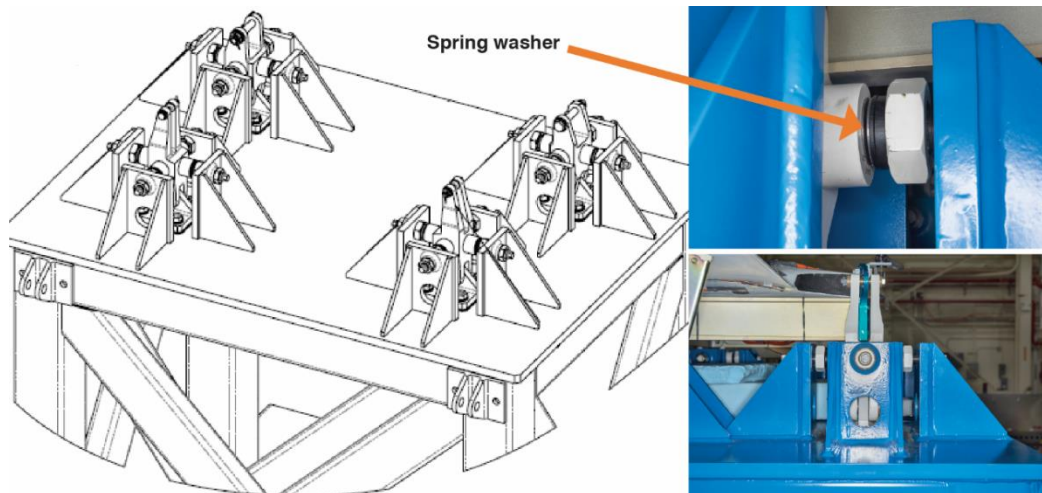
Fig. 13. The X-57 wing mount attachment and spring washer.

Fig. 14. The X-57 wing cruise motor and high-lift motor simulators.
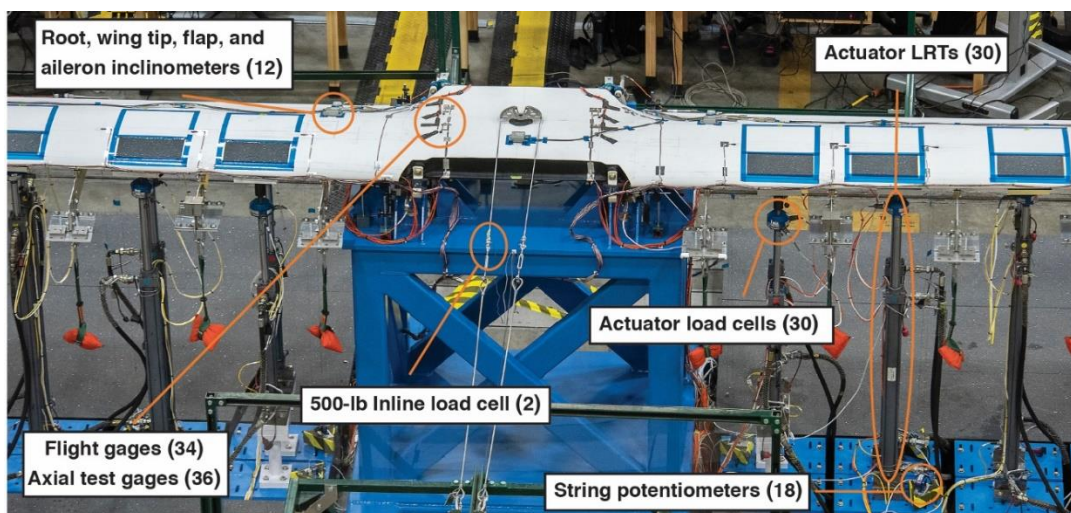
Fig. 15. The X-57 wing test instrumentation.

Fig. 16. The X-57 wing hydraulic upload testing.

Fig. 17. The X-57 wing shot-bag download testing at maximum load.

Fig. 18. The X-57 wing hydraulic upload testing with display stations.
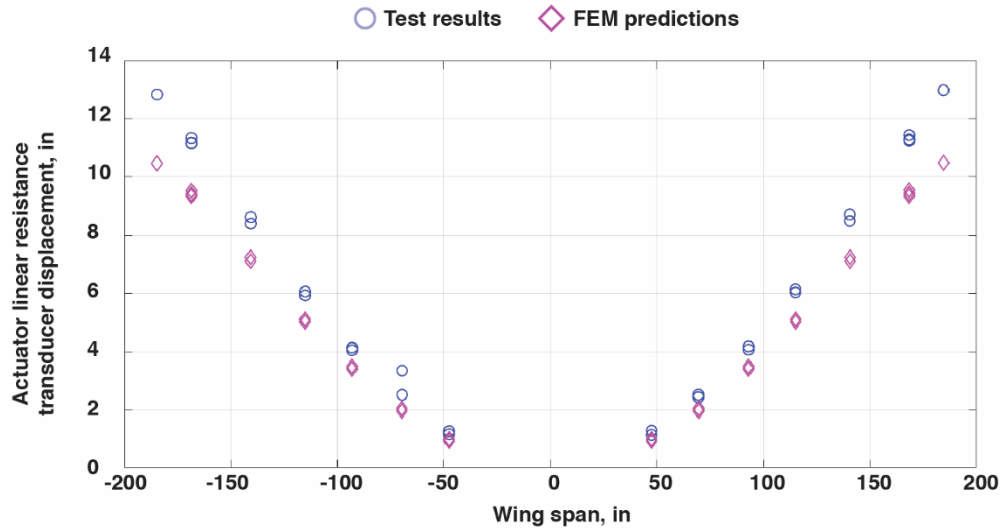
Fig. 19. The X-57 wing finite-element-model-predicted displacements compared with test results.
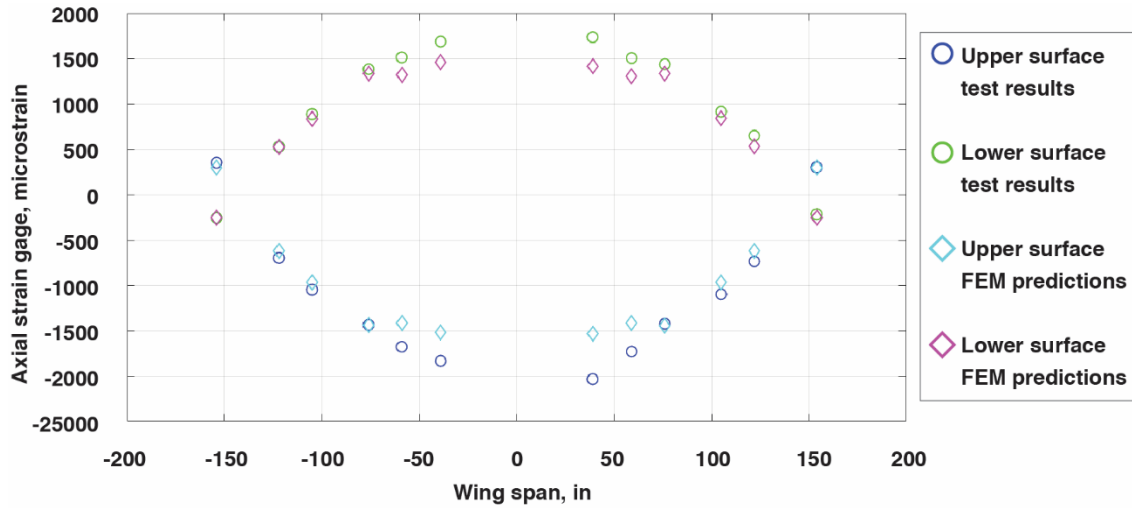
Fig. 20. The X-57 wing finite-element-model-predicted axial strain compared with test results.